We are IntechOpen,
the world's leading publisher of
Open Access books
Built by scientists, for scientists

6,900
Open access books available

185,000
International authors and editors

200M
Downloads

154
Countries delivered to

Our authors are among the

TOP 1%
most cited scientists

12.2%
Contributors from top 500 universities

Interested in publishing with us?
Contact book.department@intechopen.com

Numbers displayed above are based on latest data collected.
For more information visit www.intechopen.com

Metal Particle-Surface System for Plasmonic Lithography

V. M. Murukeshan, K. V. Sreekanth and Jeun Kee Chua
School of Mechanical and Aerospace Engineering, Nanyang Technological University
50 Nanyang Avenue,
Singapore 639798

1. Introduction

Optical (Photo) lithography has played a significant role in almost every aspects of modern micro-fabrication technology in the recent years. It has initiated transistor revolution in electronics and optical component developments in photonics. Advances in this field have allowed scientists to improve the resolution of the conventional photolithographic techniques, which is restricted by the diffraction limit [Okazaki, 1991]. To overcome this problem and to reduce the critical dimension, several solutions were introduced. New research suggests that we may be able to develop new low cost photolithographic technique beyond the diffraction limit. The minimum critical dimension (half-pitch resolution) achievable by photolithography (Optical projection lithography) is given by $CD_{half-pitch} = k_1 \lambda / NA$, where λ is the incident source wavelength, NA is the numerical aperture of projection optics of the system and k_1 is a constant value as a indication of the effectiveness of the wavefront engineering techniques. To reduce the half-pitch resolution, critical dimension equation demands either to decrease the wavelength of illumination light source or to increase the numerical aperture of projection system. Or in short, fabrication of sub-100nm features generally imposes the requirement of shorter wavelength laser sources.

In this context, the critical challenges that hinder the resolution enhancement approaches are (i) lack of availability of suitable ultra-short wavelength lasers, and (ii) the unavailability of suitable optics and materials such as photoresist for use at suitable wavelengths. Recently, techniques like extreme ultraviolet lithography (EUV) [Gwyn et al., 1998] and X-ray lithography [Silverman, 1998] have been proposed for nanofabrication overcoming the diffraction limit. Here, the illumination wavelength is reduced to the extreme UV (smaller wavelength) to get smaller features. Another reported technique is the immersion lithography in which numerical aperture of the imaging system is increased by inserting high index fluids (prism or liquid) between last optical component and wafer surface [Wu, et al., 2007]. But this technique is either limited by air absorption or availability of high index fluids. Approaches such as electron-beam lithography can also be used to overcome diffraction limit, but these are serial process and cannot be used for high throughput [Chen et al., 2005]. Imprint lithography is another option to improve the resolution beyond the diffraction limit [McAlpine et al., 2003]. Nanometer scale features are possible by stamping a

template on a thin polymer film and it can also generate sub-50nm features by integrating laser beam with AFM, NSOM and transparent particles. The main disadvantages of this technique are: (i) the leveling of the imprint template and the substrate during the printing process, which determine the uniformity of the imprint results, and (ii) slow process speed, which limits their applications in industry. The laser interference lithography (LIL) can be used to fabricate high speed and large area period nanostructures [Prodan et al. 2004]. The basic principle is the interference of coherent light from a laser source to form a horizontal standing wave pattern in the far field, which can be recorded on the photoresist.

Recently near-field lithography techniques have been proposed to overcome the diffraction limit for nanofabrication. One of the emerging areas of research is the scanning probe lithography in which the Scanning Tunneling Microscope (STM) or Atomic Force Microscope (AFM) can be used to pattern nanometer scale features, by the introduction of laser beam in to a gap between an AFM or STM tip and substrate surface with tip scanning over the surface [Jersch, 1997]. But they have stringent limitations with respect to certain materials and effectiveness applies only for certain ambient conditions. Evanescent wave lithography (EWL) is one of the near field interference lithography technique to achieve nano-scale feature at low cost [Blaikie & McNab, 2001; Chua et al., 2007]. It can create a shorter wavelength intensity pattern in the near field of diffraction grating or prism when two resonantly enhanced, evanescently decaying wave superimposed. It provides good resolution, but is limited by low contrast and short exposure depth. These problems can be subdued to a great extent by surface plasmon resonance phenomena due to their characteristics of enhanced transmission in the near field [Ebbesen et al., 1999].

Plasmonic lithography is an emerging area of near field photolithography techniques by which nano resolution features can be fabricated beyond the diffraction limit at low cost [Srituravanich et al., 2004]. Surface plasmon polaritons are electromagnetic waves that propagate along the surface of a metal [Raether, 1988]. Surface plasmon resonances in metallic films are of interest for a variety of applications due to the large enhancement of the evanescent field at the metal/dielectric interface. Hence plasmonic lithography has achieved much progress in the last decade, because it provides us a novel method of nanofabrication beyond the diffraction limit. It can provide high resolution, high density, and strong transmission optical lithography, which can be used to fabricate periodic structures for potential applications such as biosensing, photonic crystals, and high density patterned magnetic storage. Many research groups have already demonstrated that sub-100nm resolution nano structures can be fabricated using plasmonic lithography techniques.

The surface plasmon interference nanoscale lithography based on Kretschmann-Raether attenuated total reflection (ATR) geometry has been proposed numerically [Guo et al. 2006; Lim et al. 2008]. Moreover, a near field interference pattern can be formed by using metallic mask configuration that can generate surface plasmon for periodic structure fabrication [Shao & Chen, 2005; Luo & Ishihara, 2004; Liu, 2009]. In all the above mentioned works, surface plasmon can make a certain pattern on the photoresist layer when the incident p-polarized light passes through a prism or thin metallic mask. However, most of these reported techniques demands the fabrication of fine period mask grating and found to be not cost effective. The recent thrust in this challenging area focuses on exploring novel concepts and configurations to meet the sub-30nm nodes forecasted for the next decade and beyond.

In this chapter, the focus will be on a new plasmonic lithography concept for high resolution nanolithography based on the excitation of gap modes in a metal particle-surface system.

The principle, the excitation of gap modes in a metal particle-surface system and excitation of surface plasmon polaritons mediated by gap modes are illustrated and analyzed numerically from a lithography point of view. In Sect.2, the characteristics of gap modes are discussed on the basis of electromagnetic theory of a metal particle placed near to a metal surface. The concept of gap modes excited plasmonic lithography configuration has been presented in Sect.3 after giving a brief overview on conventional plasmonic lithographic configurations. A detailed analysis on the variation of electric field distribution with various parameters is numerically illustrated in Sect.4. To compute the positional development rates of photoresist domain in response to the normalized intensity profile, a modified cellular automata model is employed. In sect.5, the theoretical analysis of proposed models, followed by resist profile cross section obtained through this proposed concept is discussed. The chapter concludes in Sect.6 with a discussion on the future direction of the proposed concept and related research challenges.

2. Gap modes in metal particle-surface system

At the nanoscale, mainly electric oscillations at optical frequency contribute the optical fields, but the magnetic field component doses not contribute significantly due to weak field component. The existences of localized optical modes on dimensions much smaller than the optical wavelength are responsible for such fields to concentrate and support the nanostructured materials [Stockman, 2008]. These energy concentrating modes are called surface plasmons (SPs) and it is well known that a system should contain both negative and positive dielectric permittivities to support surface plasmons. The shape of the metal nanoparticle and metal surface thickness is an important factor for the surface plasmon resonance. A thin metal surface is associated with surface plasmon polariton (SPP) modes, which are coupled modes of photons and plasmons [Reather, 1988]. Since the SPP modes are nonradiative electromagnetic modes, to excite them the incoming beam has to match its momentum to that of the plasmons. It is possible by passing the incident photons through a bulk dielectric layer to increase the wavevector component and achieve the resonance at the given wavelength. But a fine metal particle is associated with localized surface plasmon (LSP) modes, which are collective oscillations of the conduction electrons in a metal nanoparticle [Kreibig & Vollmer, 1995]. The LSP modes can be excited directly by incident photons since they are radiative electromagnetic modes.

What happens when a system consisting of a fine metal particle placed near to a metal surface? An electromagnetic interaction between LSP modes associated with metal nanoparticle and SPP modes associated with metal surface is possible. This interaction plays an important role to enhance the light emission from metal-insulator-metal tunnel junction, mediated by metal nanoparticles [McCathy & Lambe, 1978; Adams & Hansma, 1979]. Due to this electromagnetic interaction there exist new types of localized electromagnetic normal modes, called gap modes in the space between the nanoparticles and the surface [Rendell et al. 1978; Rendell and Scalapino, 1981]. Figure 1 represents an isolated metal sphere (Al) of dielectric function $\varepsilon(\omega)$ embedded in surrounding medium (SiO$_2$) of dielectric function ε_m, is placed close to a metal surface (Ag). The retardation effects of electromagnetic fields can be neglected when the radius (R) of the sphere is small and resonant frequencies corresponding to the excitation of LSP are expressed by $\varepsilon(\omega) = -\varepsilon_m(l+1)/l$, where $l = 1, 2, ...$ is an integer [Boardman, 1982]. If the sphere is much smaller than the wavelength of the incident light, the dipole mode with $l = 1$ is mainly excited.
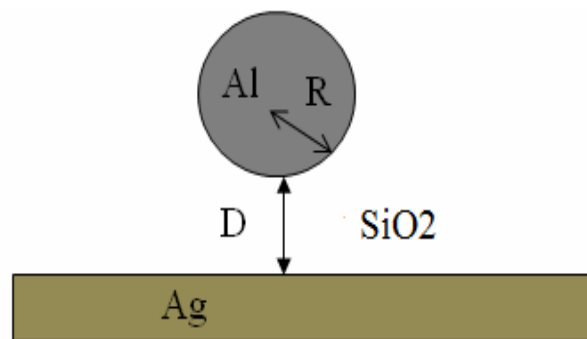
Fig. 1. Schematic diagram of the metal particle-surface system: Al nanosphere of radius R is placed at a distance D from the Ag surface.

Theoretically, this concept can be explained by approximating the LSP modes as a dipole and considering its interaction with image dipole induced inside the metal surface. This dipole-dipole interaction may greatly modify the LSP mode and hence the resonance frequency and field distribution. In other way, new electromagnetic modes are expected to appear by change in symmetry of the system. It means the spherical symmetry of the isolated sphere translate to cylindrical symmetry for a sphere-surface system. These modes also correspond to polarization modes parallel and perpendicular to the symmetry axis [Hayashi, 2001]. When the particle-surface distance is sufficiently small (D/R<1), this system can support a series of gap modes and the electric field becomes more and more localized at the gap between the particle and the surface. When the gap mode is excited, the intensity of the electric field is enhanced relative to that of the excitation field and these modes are believed to play an important role in the light emission process. It is reported that the maximum enhancement factor is larger than that achieved with an isolated particle (LSP excitation) or a surface alone (SPP excitation) system [Hayashi, 2001].

The metal particle-surface system supposed to find variety of potential applications in near field optics, although the roles played by the gap modes have not yet been fully explored. One of the promising applications in scanning tunneling microscope (STM) in which the tunneling current are excited by gap modes [Johansson et al., 1990]. In STM, SPP modes in a metallic surface are excited by ATR method. To obtain images with high lateral resolution, the intensity of the reflected and scattered light can be enhanced by placing a sharpened metallic tip very close to a surface. Theoretical treatments of this problem is already reported, in which tip is often modulated by a sphere [Madrazo et al., 1996]. The direct evidence of the existence of gap modes is experimentally demonstrated by Hayashi's group [Hayashi, 2001]. They performed a systematic absorption measurement on Ag island particles placed above an Al surface and realized strong localization and strong enhancement of electromagnetic field under the conditions of resonant excitation of gap modes.

3. Plasmonic lithography configurations

The two well known methods proposed to excite surface plasmons on a thin film and subsequent realization of plasmonic lithography are based on configurations using prism coupling (Kretschmann) and grating coupling (Metal grating mask).

3.1 Kretschmann configuration

Kretschmann (Prism based) configuration is a well known method used to excite surface plasmon polariton, performed with the evanescent field generated by ATR principle and thereby enabling SP interference. Figure 2 represents the SP interference lithography technique using Kretschmann configuration, in which the upper layer is a high refractive index isosceles triangle prism. The coated thin metal layer is at the bottom surface of the prism, which is in contact with the photoresist layer on a substrate.
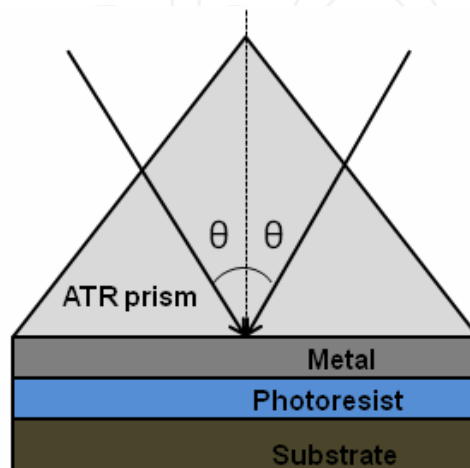
Fig. 2. Schematic diagram of Kretschmann configuration

3.2 Metal grating mask based configuration
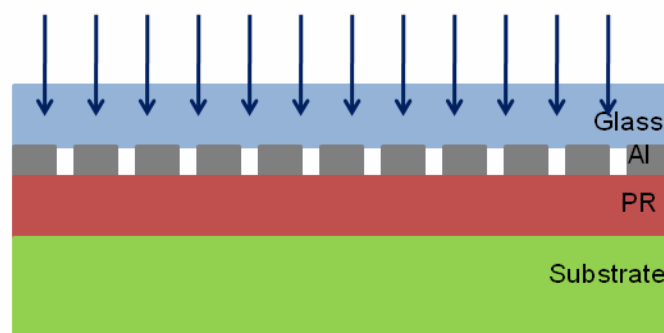
Fig. 3. Metal grating mask based configuration

Metal mask grating based configuration is a commonly used technique for plasmonic lithography. As distinct from a Kretschmann scheme, the mask grating based scheme is much more compact. In this configuration, the period of the grating can be several times greater than the period of the expected interference pattern and interference of various diffraction orders generate the SP interference pattern on the photoresist layer. The optical near field of metallic mask can produce fine features with subwavelength scale resolution. The schematic of plasmonic lithography configuration using metal mask is shown in Fig.3. It consists of metal mask, which can be fabricated on a thin quartz glass by electron-beam lithography and lift off process. And mask is brought into intimate contact with a photoresist coated on a silica substrate. Light is incident normally from the top and light tunnels through the mask via SPP and reradiates in to the photoresist.

3.3 Gap modes excited configuration

Schematic diagram in Fig. 4 represents the plasmonic lithography configuration based on the excitation of gap modes in metal particle-surface system. It consists of a high refractive index thin dielectric layer kept below the incident prism medium, which is in contact with periodic Al metal nanospheres. Period of Al nanosphere array is taken as 24 nm. These Al nanospheres are embedded in a lower refractive index surrounding medium (SiO₂). A thin Ag metal film is coated at distance D from the Al nanospheres in the surrounding medium and in contact with photoresist layer on a silica substrate. The diameter of Al nanospheres is taken as 20nm and thickness of Ag film is 10 nm.
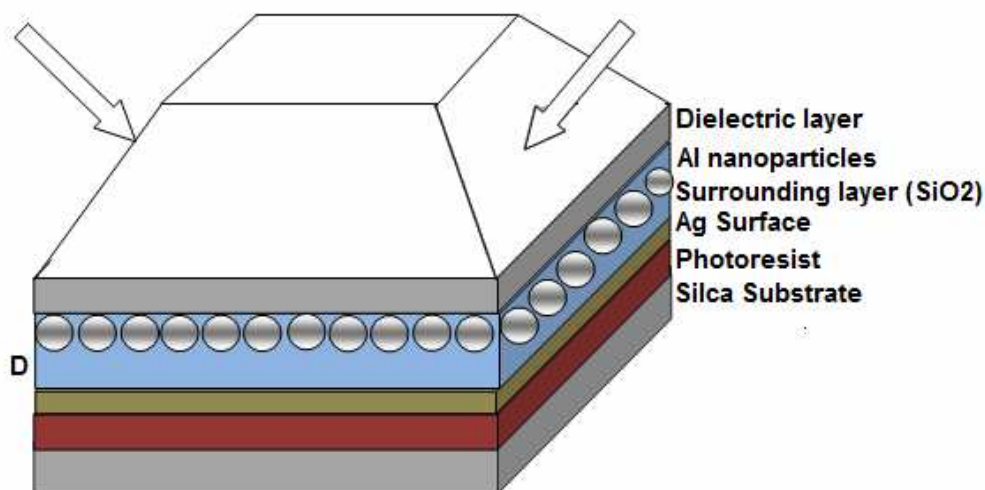

Fig. 4. Schematic diagram of gap modes excited plasmonic lithography configuration (Adapted from Ref. [V. M. Murukeshan and K. V. Sreekanth, Opt. Lett. 34, 845-847 (2009)])

The basic idea of the technique is that the excited gap modes above the metal surface can greatly enhance the surface plasmons on the metal surface and superposition of two excited SP modes generates the interference patterns on the photoresist layer. By applying the appropriate boundary condition at the metal surface/photoresist interface, the dispersion relation for surface plasmon polariton is described as [Raether, 1988],

$$k_{SP} = k_x = \frac{\omega}{c} \sqrt{\frac{\varepsilon_m \varepsilon_d}{\varepsilon_m + \varepsilon_d}} \tag{1}$$

where ω the excitation frequency, c is the speed of light in vacuum, ε_m is the complex dielectric constants of wavelength dependent metal and ε_d is the dielectric constants of photoresist layer. The wavevector of surface plasmon wave becomes significantly larger than that of the incident light wavevector, when the real parts of ε_m approaches - ε_d. At this condition, the wavelength of the excited SPs get normally shorter compared to the wavelength of illumination light. Furthermore the modes responsible for the field distribution could be weakly coupled gap modes of single particle-film systems.

4. Electric field distribution

The finite difference time domain (FDTD) method is used to predict the light intensity distribution on the photoresist layer. The simulation region is terminated with perfectly

matched layer (PML) boundary condition on the boundaries perpendicular to the propagation direction of the light and Bloch boundary condition on the other boundaries. The refractive index of the upper prism, dielectric layer and photoresist layer are 1.745 (NLK8 glass), 1.939 (NLAF31A glass) and 1.53 (AZ9200 from AZ Electronic Material) respectively. The dielectric layer thickness is assumed to be 90nm. The wavelength of p-polarized light is taken as 427 nm (as shown in Fig. 5) and incident resonant angle is 56° at this wavelength. The complex dielectric constants of aluminium and silver at this wavelength are -26.728+5.8i and -5.082+0.7232i respectively [Palik, 1985].
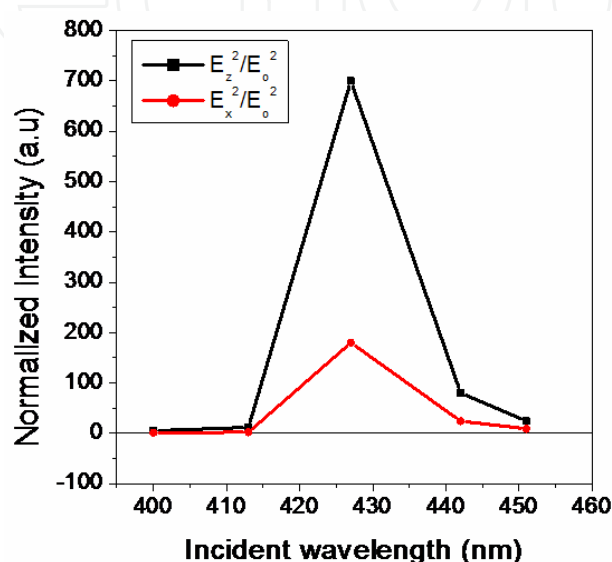
Fig. 5. Variation of normalized intensity with incident wavelength.

The normalized intensities measured along metal surface/photoresist interface as a function of incident wavelengths is shown in Fig. 5, where incident angle is assumed to be 56°. It is evident from the figure that intensity distribution is possible for a band of wavelength and maximum intensity is obtained when incident resonant wavelength is 427 nm. It is also evident that there is a large intensity variation when incident wavelength varies from 413 nm to 442 nm. It could be due to large gap modes excitation at that wavelength range and peak at 427 nm. When two p-polarized 427 nm illumination light beam incident at the dielectric layer/nanosphere interface, the field intensity distribution developed on the photoresist surface is shown in Fig.6. Figures 6(a) and 6(b) respectively shows the field distribution of E_x and E_z components, when particle-surface distance D=0 nm. And Figures 6(c) and 6(d) respectively represents that of conventional prism based configuration (shown in Fig.2) in which high refractive index prism with an Ag metal film coated onto the bottom side and in contact with photoresist layer on a silica substrate. Here the thickness of the Ag film is taken as 20 nm and remaining parameters are same as the proposed configuration. It should be noted that Ag film thickness of 10 nm for proposed configuration and 20 nm for the prism layer configurations are the required respective Ag film thickness for obtaining maximum intensity.

Figure 7 represents the normalized intensity variation, ($|E|^2 / |E_0|^2$) where E_0^2 is the incident intensity) with decay direction. Here Z-axis is considered as the decay direction. The
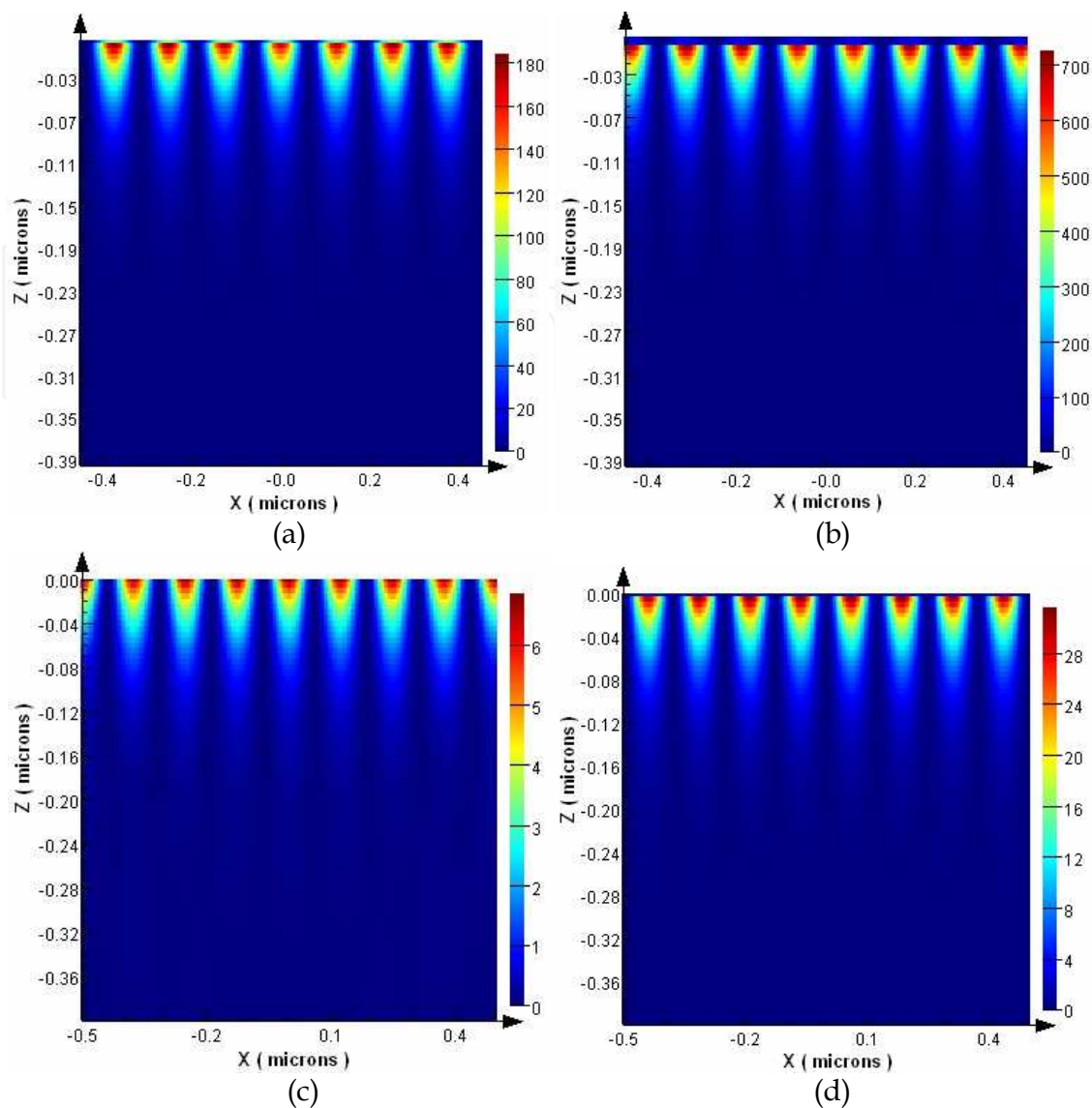
Fig. 6. Electric field distribution of the interference pattern generated by the field components on the photoresist layer (a) E_x (b) E_z of proposed configuration and (c) E_x, (d) E_z of prism based configuration. (Adapted from Ref. [V. M. Murukeshan and K. V. Sreekanth Opt. Lett. 34, 845-847 (2009)])

exposure fields E_z and E_x represents the longitudinal and transverse components respectively. The E_z component is much stronger than the E_x component and these components have $\pi/2$ phase difference in both configurations. The electric field distribution show that interference patterns with approximate periodicity of 120 nm is formed at the interface for both configurations. From the Fig. 6 and Fig.7, it is evident that the proposed configuration gives high electric field distribution compared to conventional prism based configuration. The intensity transmission calculated at metal surface/ photoresist interface is 4% for conventional prism based configuration compared to that of the proposed configuration. Therefore the maximum enhancement factor is much larger for this configuration compared to that achieved with conventional prism based configuration. From the Fig. 7, it is clear that the exposure depth above 350 nm is achieved for the proposed scheme, but prism based configuration gives around 250 nm. The fringe visibility

or contrast can be expressed as $V = (I_{max} - I_{min}) / (I_{max} - I_{min})$, where $I_{max} = E_z^2$ and $I_{min} = E_x^2$. The intensity contrast calculated is around 0.90 for both configurations within the exposure depth of 200 nm, which is sufficiently high for the realization of interference patterns and much higher than the exposure threshold of common negative optical resists.
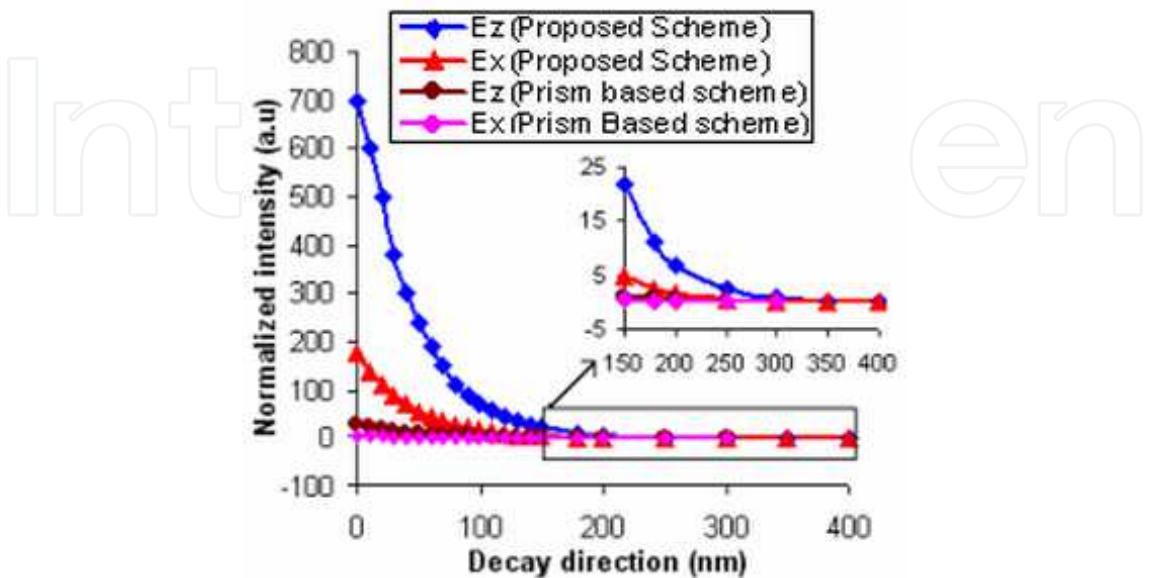

Fig. 7. Normalized intensity variation with decay direction. (Adapted from Ref. [V. M. Murukeshan and K. V. Sreekanth, Opt. Lett. 34, 845-847 (2009)])
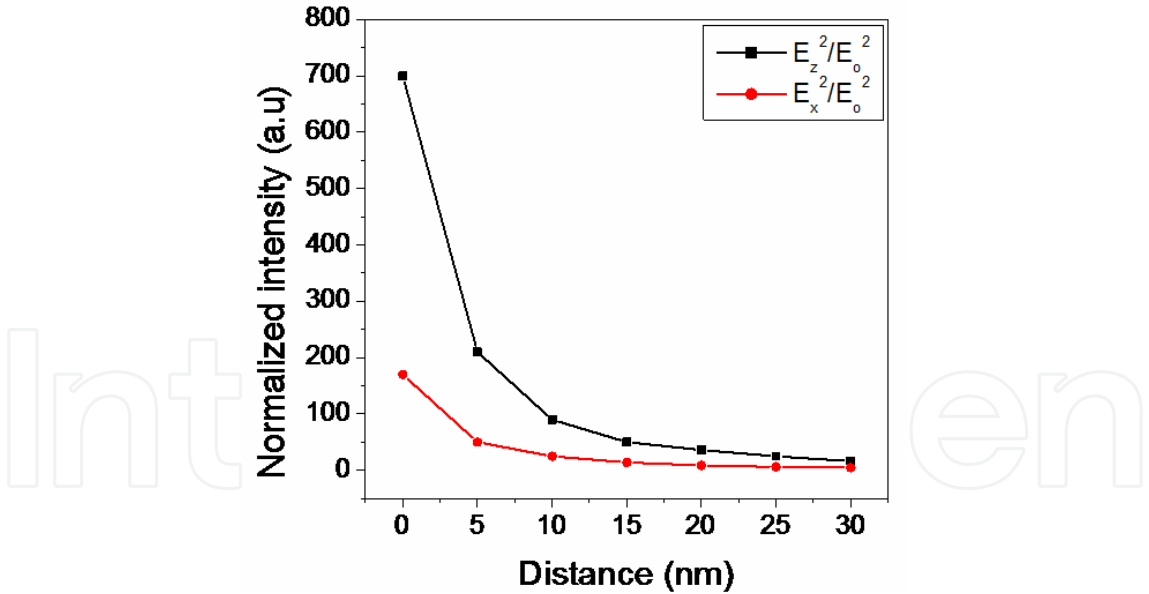
Fig. 8. Normalized intensity variation as a function of metal particle-surface distance (D). (Adapted from Ref. [V. M. Murukeshan and K. V. Sreekanth, Opt. Lett. 34, 845-847 (2009)])

The metal particle-surface distance (D) is an important factor for the gap mode excitation. Therefore the variations of normalized intensities with D need to be analyzed. Figure 8 shows the variation of normalized intensities of E_x and E_z component calculated along metal surface/photoresist interface as a function of metal particle-surface distance D. The distance D is varied from 0 to 30 nm and interference patterns are observed in all cases. From the

figure it is clear that when D=0 nm, maximum intensity is obtained and both intensity component decreases when distance increases. It is also evident from the figure that there is a large intensity variation when D varies from 0 to 5 nm. That is when D decreases; the field becomes more and more localized at the gap between the particle and the surface. The localization and excitation of electromagnetic normal modes are caused by resonant excitation of electromagnetic normal modes of the particle-surface system. It correlates well with theory.

5. Resist dissolution process

A modified cellular automata (CA) scheme for simulating resist dissolution during the development process is employed to compute the positional development rates of the photoresist domain in response to the normalized intensity profile (value of 1 mW/cm² for the unit normalized intensity value is adopted).

5.1 Theoretical model

Various forms of CA numerical techniques have been reported for simulating the photoresist development process in both the 2D and 3D spatial domain, showing good agreement between the simulated and experimental results [Karafyllidis, et al 2000; Scheckler, et al 1993]. During the development process, the developing reagent dissolves the exposed photoresist in an isotropic manner. In addition to the proven level of accuracy, the CA technique is straightforward in implementation as it allows the user to employ regular and uniform spatial and temporal discretization in modeling the physical system.

A modified three dimensional CA algorithm that follows closely, to the one proposed by Karafyllidis [Karafyllidis, 1999] is employed here. The exposed photoresist domain is divided into identical cubic CA cells, each with edge length a. Unlike previous works, the algorithm implemented here considers all the neighboring cells in the computation sub-domain when solving for the local state of the concerned cell. The local state of each CA cell is defined as the ratio of its etched volume to its total volume and the respective computation sub-domain is illustrated in Fig. 9. Based on Fig. 9, the amount of each cubic cell set at the position (i, j, k), dissolved at time instant t by its local state, $C_{i,j,k}^t$ this is defined as,

$$C_{i,j,k}^t = h_{diss}/a \qquad (2)$$

where h_{diss} is the height dissolved in the development process. Based on the definition, the initial value for $C_{i,j,k}^t$ is assigned zero and when the computed value for which exceeds one, a value of one would be assigned. We further introduce the differential cell state terms, dC_{adj}, dC_{edg} and dC_{vtx}. These represent the change of the central cell state(cell for which the state to be solved) due to the flow of the developer from adjacent, edge and vertex cells positions at the new time instance, after one time step of dt from the time instance t_0.

An adjacent neighboring cell shares one face with the central cell, an edge neighboring cell shares an edge with the central cell and a vertex neighboring cell shares a corner vertex with the central cell. As such, the central cell state at the new time instance is defined here as,
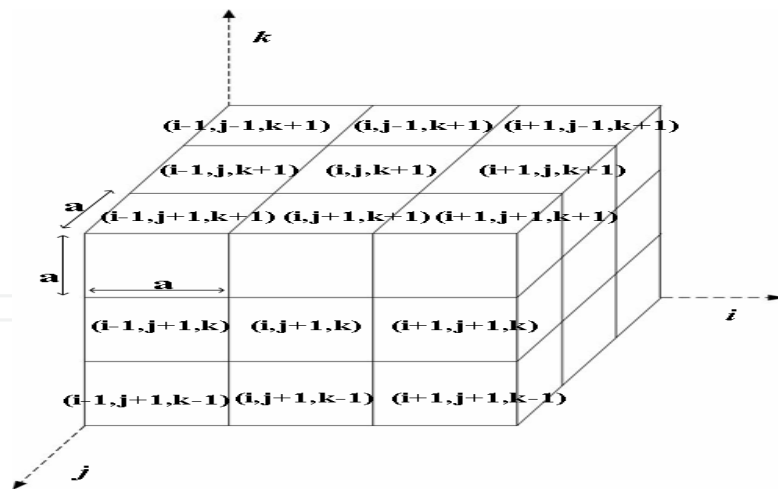
Fig. 9. The neighbourhood of the (i, j, k) cell. (Adapted from Ref. [Murukeshan et al, Opt. Eng. 47, 129001 (2008)])

$$C_{i,j,k}^{t_o+dt} = C_{i,j,k}^{t_o} + dC_{adj}^{dt} + dC_{edg}^{dt} + dC_{vtx}^{dt} \tag{3}$$

Assuming that the dissolution rate of the central cell to be $R_{i,j,k}$, terms would be defined as follow,

$$dC_{adj}^{dt} = \frac{\left(\left(C_{i+1,j,k}^{t_o} + C_{i-1,j,k}^{t_o} + C_{i,j+1,k}^{t_o} + C_{i,j-1,k}^{t_o}\right) + B_{i,j,k+1}^{t_o} + B_{i,j,k-1}^{t_o}\right)R_{i,j,k}dt}{a} \tag{4}$$

$$
\begin{aligned}
dC_{edg}^{dt} = \gamma_{edg}\bigg(&\left(C_{i+1,j+1,k}^{t_o} + C_{i-1,j+1,k}^{t_o} + C_{i+1,j-1,k}^{t_o} + C_{i+1,j-1,k}^{t_o}\right)\cdots \\
&+B_{i+1,j,k+1}^{t_o} + B_{i-1,j,k+1}^{t_o} + B_{i,j+1,k+1}^{t_o} + B_{i,j-1,k+1}^{t_o}\cdots \\
&+B_{i+1,j,k-1}^{t_o} + B_{i-1,j,k-1}^{t_o} + B_{i,j+1,k-1}^{t_o} + B_{i,j-1,k-1}^{t_o}\bigg)\frac{2R_{i,j,k}^2 t_o dt}{a^2}
\end{aligned} \tag{5}
$$

$$
\begin{aligned}
dC_{vtx}^{dt} = \gamma_{vtx}\bigg(&B_{i+1,j+1,k+1}^{t_o} + B_{i-1,j+1,k+1}^{t_o} + B_{i+1,j-1,k+1}^{t_o} + B_{i+1,j-1,k+1}^{t_o}\cdots \\
&+B_{i+1,j+1,k-1}^{t_o} + B_{i-1,j+1,k-1}^{t_o} + B_{i+1,j-1,k-1}^{t_o} + B_{i+1,j-1,k-1}^{t_o}\bigg)\frac{3\sqrt{3}}{8a^3}R_{i,j,k}^3 t_o^2 dt
\end{aligned} \tag{6}
$$

where $B_{I,J,K}^{t_o}$ is defined as,

$$B_{I,J,K}^{t_o} = \begin{cases} 1 & C_{I,J,K}^{t_o} = 1 \\ 0 & \text{otherwise} \end{cases} \tag{7}$$

where I may represents $i - 1$, i, or $i+1$ and likewise for J and K. As shown in Eq. (4) to Eq. (6), the binary switch function is implemented at those cell positions with $K = k - 1$ or $K = k + 1$. The hypothesis for the choice of implementation is that the central cell would not be exposed to developer from the higher or lower cell positions until the resist elements occupying those positions are completely dissolved. The time step, dt is defined as, $a/4R_{max}$ where R_{max} refers to largest elemental development rate value in the simulation domain. In

this work, the terms γ_{edg} and γ_{vtx} are parameters used to model the indirect flow of developer from the edge cell positions and from the vertex cell positions. The best values for γ_{edg} and γ_{vtx} would be shown and discussed in the later section.

5.2 Homogenous development rate test

The modified 3D CA model is evaluated using a homogeneous etch-rate distribution function [Karafyllidis, 1999] to determine the values of γ_{edg} and γ_{vtx} in Eq (5) and Eq (6) and their effectiveness to describe the effects from the edge and vertex cells. The cells are assigned the same development rate value. At the beginning of the simulation, all the cell states are assigned value of zero except for the one at the centre of the top surface. For the CA model proposed here, the optimum γ_{edg} and γ_{vtx} values would be searched so that the generated profile has the closest conformity to that of a hemispherical crater. For this purpose, we adopt a statistical approach that is explained with the aid of Fig. 10.
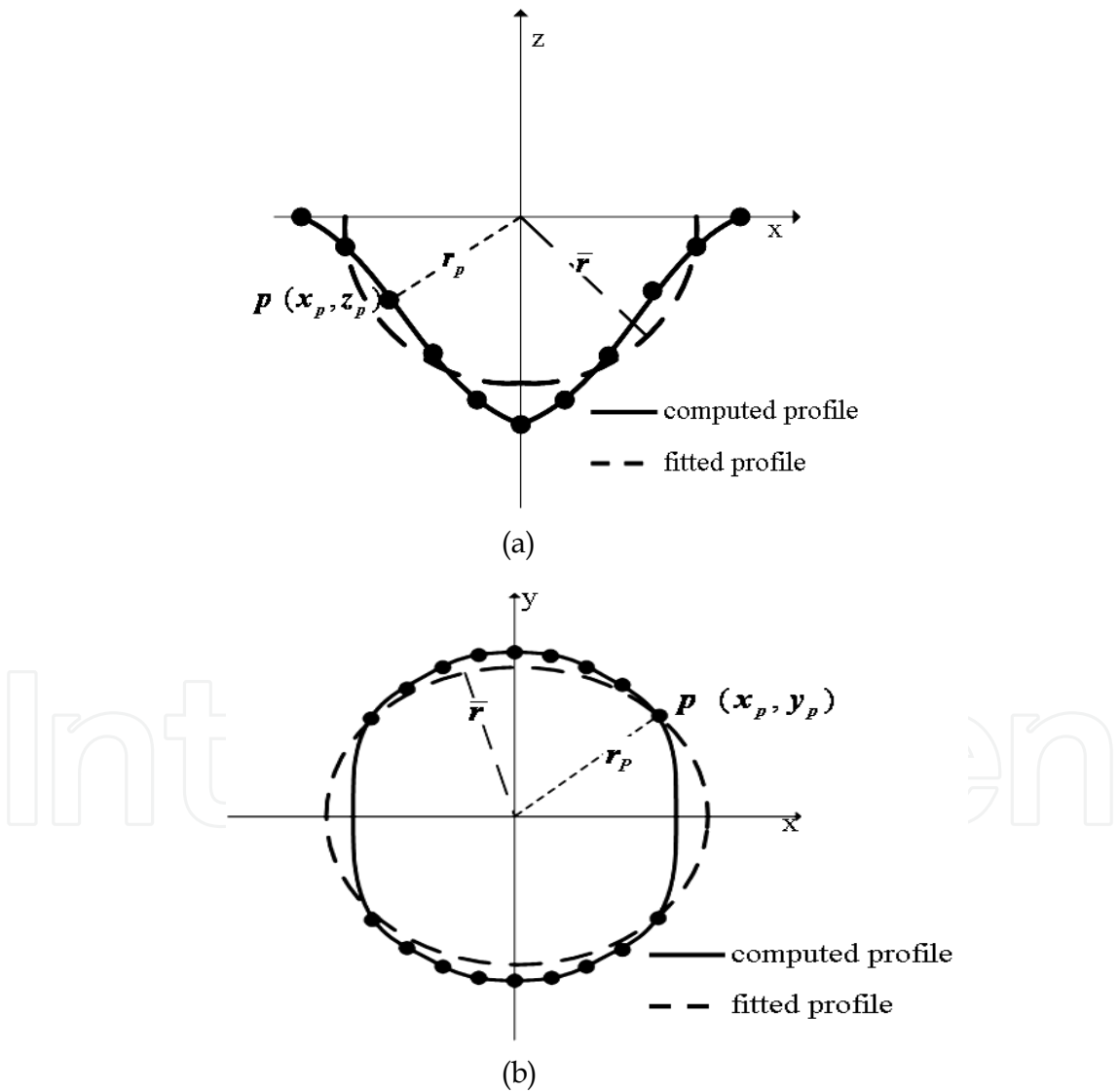

(a)

(b)

Fig. 10. Computed and fitted profiles for (a) a cross section and (b) the top of the generated hemispherical crater in the homogeneous development rate test. (Adapted from Ref. [Murukeshan et al, Opt. Eng. 47, 129001 (2008)])

Each computed boundary point p is quantified by its distance from the origin given by $r_p = (x_p^2 + y_p^2 + z_p^2)^{1/2}$. The fitted profile is generated by assuming a semicircle for the cross-section profile and a circle for the top profile, as shown in Fig. 10(a) and 10(b), respectively. The radius of $\bar{r}$ is given by $\bar{r} = \sum_{p=1}^{N} r_p \Big/ N$, where N refers to the number of computed profile by the standard deviation σ of the computed r_p values from the $\bar{r}$ value of the fitted perfect hemisphere. A smaller σ value would infer that the computed profile has a higher conformity to a spherical profile. A range of values for γ_{edg} and γ_{vtx} are investigated to identify the combination that generate the smallest σ value. The values for γ_{edg} and γ_{vtx} are varied from 0.1 to 1.0 with coarse step size of 0.1 and with the same total number of time steps. The corresponding results are given in Fig. 11.
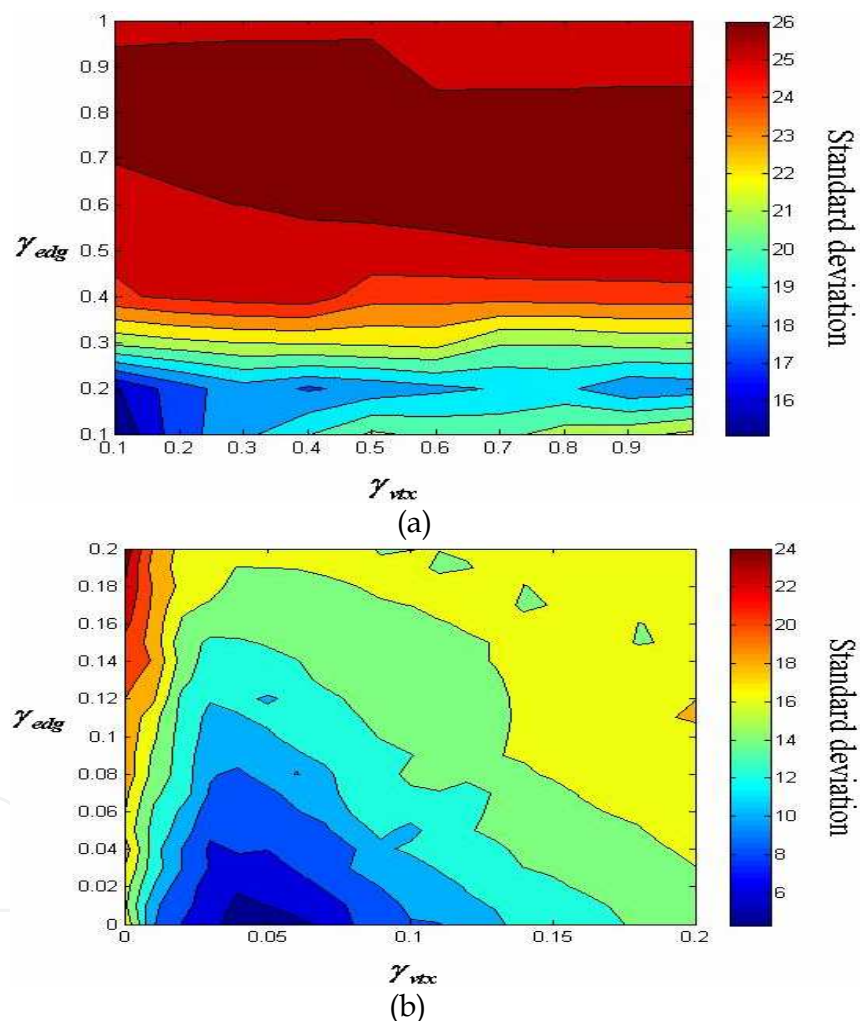

Fig. 11. Contour distribution of standard deviation with respect to coupled variation γ_{edg} and γ_{vtx}, (a) coarse (b) fine variations of γ_{edg} and γ_{vtx} values. (Adapted from Ref. [Murukeshan et al, Opt. Eng. 47, 129001 (2008)])

After identifying the possible combinations of γ_{edg} and γ_{vtx} values, the analysis is repeated, using a smaller range of values and a smaller step size of 0.001. The results in Fig. 11(b) suggest that the best γ_{edg} and γ_{vtx} values are 0 and 0.04, respectively, yielding a standard deviation value of 4.29 nm. The CA modal is simplified by employing the obtained γ_{edg} and

γ_{vtx} values shown in Eqs. (5) & (6). The results for the homogeneous development rate, shown in Fig. 12, are obtained with the optimum γ_{edg} and γ_{vtx} values.

(a)

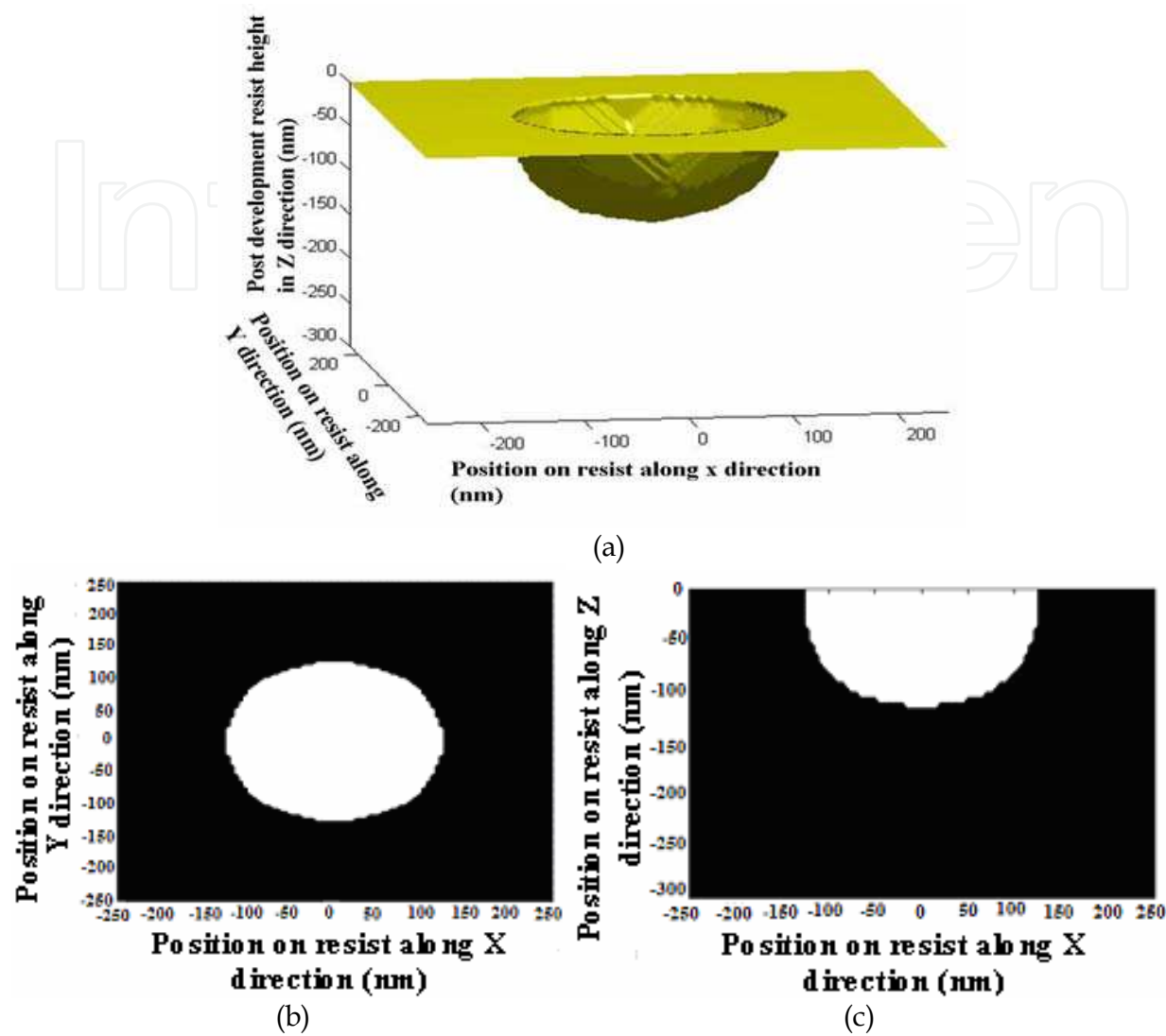(b)   (c)

Fig. 12. (a) Three dimensional perspective of the crater generated by the CA model. (b) Computed profile on the x-y plane at z=0 (c) Computed profile on the x-z plane through y=0. (Adapted from Ref. [Murukeshan et al, Opt. Eng. 47, 129001 (2008)])

The generated crater shows a reasonably good hemispherical profile. This result suggests that the proposed CA modal is reasonably accurate in simulating the isotropic nature of the resist-etching mechanism during the resist development process. Besides CA, another widely used numerical scheme for simulating resist development is the fast marching level set method formulated by Sethian and Adalsteinsson [Sethian & Adalsteinsson, 1997]. This method is efficient in handling a large computation domain and accurate in simulating resist topologies with complex geometrics, as in the case of lithography simulation for semiconductor chip fabrication.

5.3 Resist features
The modified CA modal is adopted in order to obtain the resultant resist features, as discussed in the previous sect. 5.2
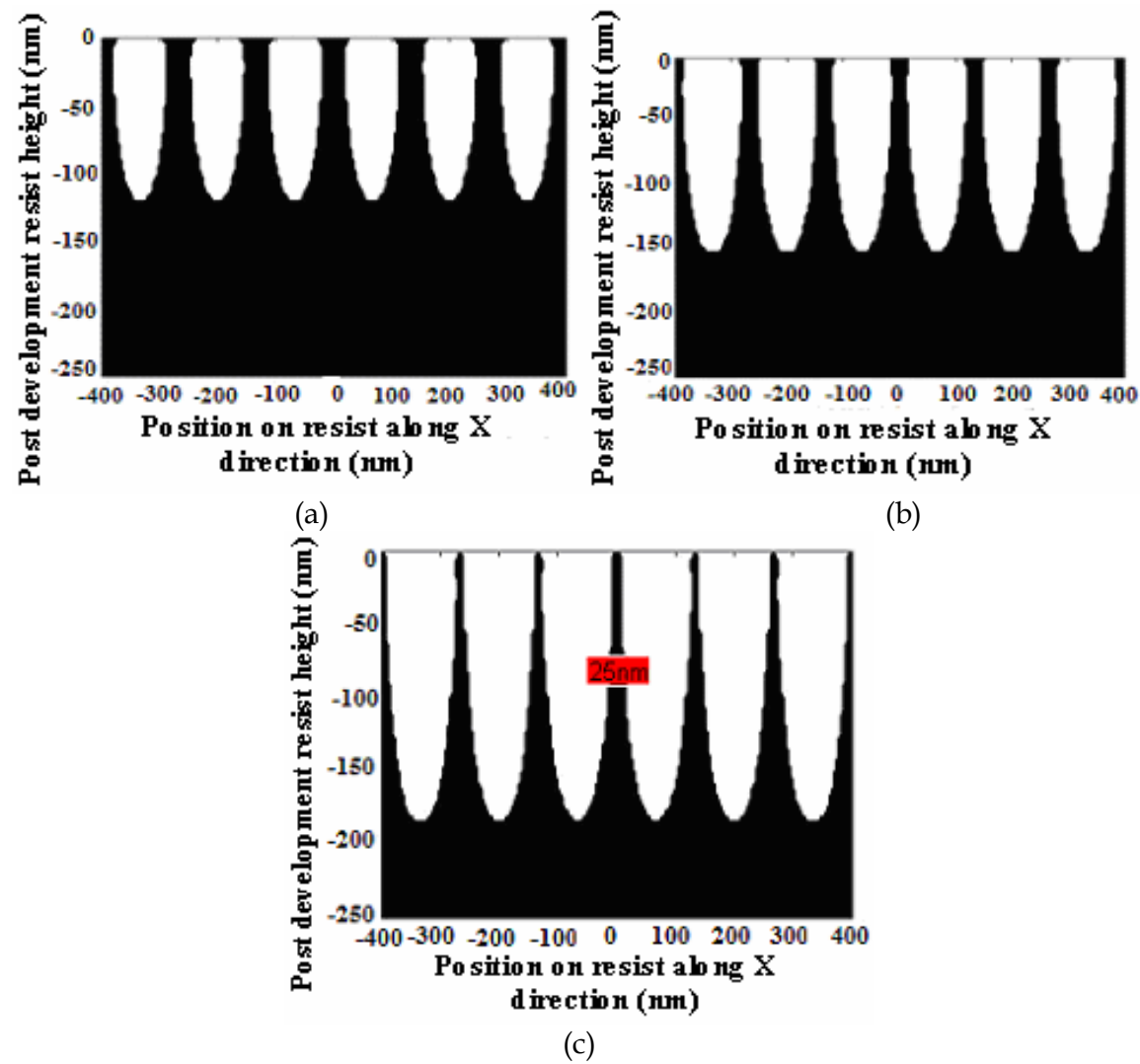
Fig. 13. 2D resist profile cross section at exposure times: (a) =50 s, (b) =100 s and (c) =150 s. (Adapted from Ref. [V. M. Murukeshan and K. V. Sreekanth, Opt. Lett. 34, 845-847 (2009)])

Figures 13 and 14 respectively show 2D and 3D resist cross-section profiles obtained on the photoresist layer by employing the proposed concepts and configuration at different exposure times. The zero value along the vertical axis corresponds to the metal/photoresist interface. The obtained result shows that with increase in exposure time, the line width of the pattern decreases and exposure depth increases. Fig.13 (c) shows that at 150 s exposure duration, the obtained line width, periodicity and exposure depth are around 25 nm, 120 nm and 180nm respectively. Therefore approximate resolution of 25 nm is achievable by this configuration, which is generally not possible with conventional prism based configuration. Also, the advantage of this configuration is that it can provide much larger enhanced fields to give shorter wavelengths of surface plasmons compared to that achieved with an isolated metal particle or a metal surface alone configuration.

6. Conclusion

A recently proposed novel plasmonic lithographic concept and methodology based on the excitation of gap modes in a metal particle-surface system is discussed in this chapter. The
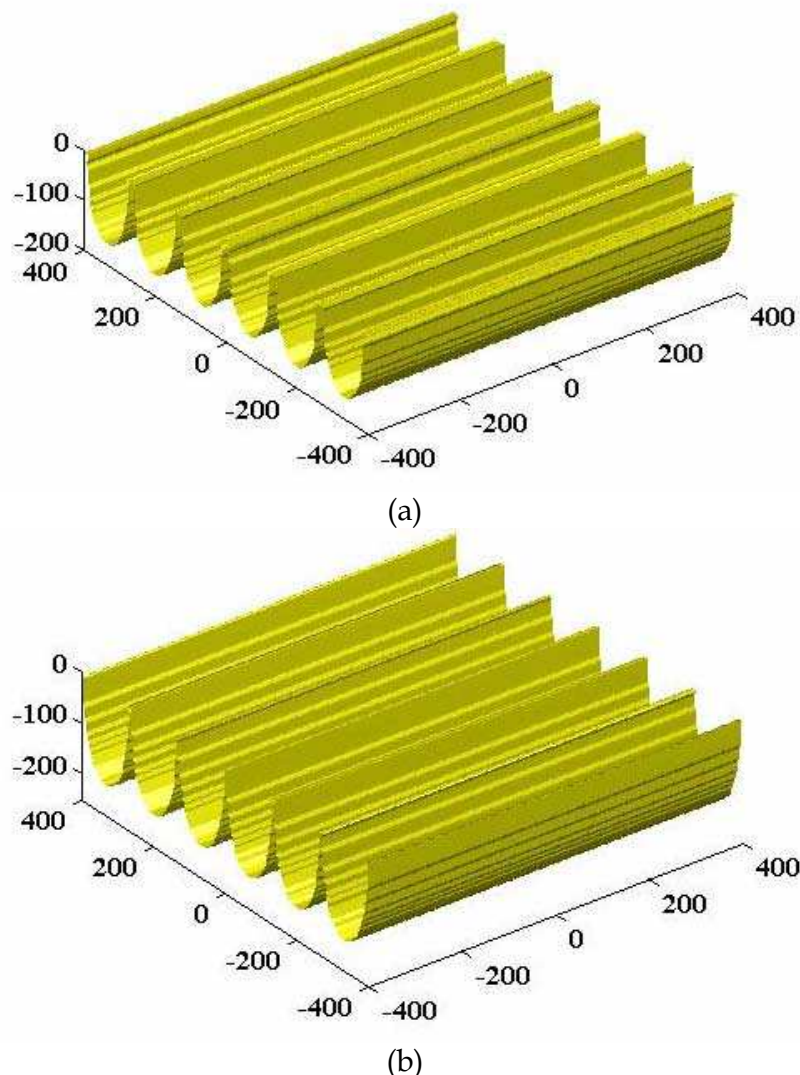
(a)

(b)

Fig. 14. 3D resist profile cross section at exposure times: (a) =100 s, (b) =150 s

proposed approach is compared with conventional configurations and illustrated numerically that the exposure depth of the pattern achieved with this configuration is much higher than that achieved with a conventional prism based configuration. The simulation result also shows that this configuration can provide strong enhanced field to give shorter wavelengths of surface plasmons to fabricate sub-25 nm size periodic structures. In order to simulate the resist removal process during the post exposure development stage, a modified CA algorithm was proposed and explained. The theoretical analysis of CA model and resist profile cross section obtained through this proposed configuration is also presented. It is expected that this lithography concept can achieve high resolution, good exposure depth and good contrast to fabricate one-dimensional periodic nanostructures for various applications including biosensors, photonic crystals, and waveguides.

It should be noted that though a dielectric sphere/dielectric surface based configuration contribute gap modes, the degree of localization and enhancement is smaller than that for a metal sphere-surface system. The experimental evidence of the proposed configuration also need to be investigated further. In a practical scenario, to fabricate high aspect ratio nanoscale features, certain requirements must be met. First, the laser output beam should

have good pointing stability. Second, a high contrast of the interference fringes must be achieved by keeping the intensity between the incident beams equal, followed by the appropriate control of their polarization state. Third, the mechanical strength of the photoresist must be high enough to withstand the capillary force exerted by fluid between the features. The capillary force is directly proportional to the aspect ratio of the features. These above mentioned potential research challenges augur well for realizing high resolution , high aspect ratio feature fabrication in the near future.

7. Acknowledgment

8. References

Adams, A.; Hansma, P.K. (1981). Light emission from small metal particles and thin metal films excited by tunneling electrons. *Phys. Rev. B*, 23, 8 3597-3601, 1550-235X.

Blaikie, R. J.; McNab, S. J.(2001). Evanescent interferometric lithography. *Appl. Opt.*, 40, 10, 1692-1698, 1539-4522.

Boardman, A.D. (1982). Electromagnetic surface modes. John Wiley & Sons Ltd, 0471100773, Chichester.

Chen, K.S.;Lin, I.K.; Ko, F. H. (2005). Fabrication of 3D polymer microstructures using electron beam lithography and nanoimprinting technologies. J. Micromech. Microeng., 15, 10, 1894-1903, 1361-6439.

Chua, J. K.; Murukeshan, V. M.; Tan, S. K.; Lin, Q. Y. (2007). Four beams evanescent waves interference lithography for patterning of two dimensional features. Opt. Exp., 15, 6, 3437-3451, 1094-4087.

Ebbesen, T. W.; Lezec, H. J.; Ghaemi, H. F.; Thio, T.; Wolff, P. A. (1991). Extraordinary optical transmission through sub-wavelength hole arrays. *Nature* (London), 391, 667-669, 1476-4687.

Gwyn, C. W.; Stulen, R.; Sweeney, D.; Attwood, D. (1998). Extreme ultraviolet lithography. *J. Vac. Sci. Technol*. B, 16, 3142-3149, 1520-8567.

Guo, X.; Du, J. ; Guo, Y.; Yao, J.(2006). Large-area surface- plasmon polariton interference lithography. *Opt. Lett,* 31,17, 2613-2615, 1539-4794.

Hayashi, S. (2001). Spectroscopy of gap modes in metal particle-surface systems, In: *Near-field optics and surface plasmon polaritons*, Kawata, S. 71-95, Springer. 978-3-540-41502-2, Berlin Heidelberg.

Jersch.J. (1997). Nanostructuring with laser radiation in the near field of a tip from a scanning forcen microscope, *Appl. Phys. A*, 64, 29-32, 1432-0630.

Johansson, P.; Monreal, R.; Appel, P. (1990). Photon emission from STM-concepts, *Phys. Rev. B,* 42, 9210, 1550-235X.

Karafyllidis, I. (1999). A three-dimensional photoresist etching simulator for TCAD, *Modeling Simul. Mater. Sci. Eng.* 7, 157-168, 1361-651X

Karafyllidis, I; Hagouel, P. I.; Thanailakis, A.; Neureuther, A. R. (2000). An efficient photoresist development simulator based on cellular automata with experimental verification. *IEEE Trans. Semicond. Manuf.* 13, 61-75, 0894-6507.

Kreibig, U.; Vollmer, M. (1995).*Optical properties of metal clusters,* Springer, 0387578366, Berlin/ Heidelberg.

Lim, Y; Kim, S; Kim, H; Jung, J; Lee, B (2008) Interference of surface plasmon waves and plasmon coupled waveguide modes for the patterning of thin film. *IEEE J. of. Quant. Elec.* 44, 305-311, 0018-9197.

Liu, Z.; Wang, Y.; Yao, J.; Lee, H.; Srituravanich, W.; Zhang, X. (2009) Broad band two dimensional manipulation of surface plasmons. *Nano Lett.*, 9, 1, 462-466, 1530-6992.

Luo, X.; Ishihara, T. (2004). Surface plasmon resonant interference nanolithography technique, *Appl. Phys. Lett.*, 84, 23, 4780-4782, 1077-3118.

Madrazo, A; Neito-Vesperinas, M. (1996). Exact calculation of Maxwell equations for a tip-metallic interface configuration: Application to atomic resolution by photon emission. *Phys. Rev. B*, 53, 3654-3657, 1550-235X.

McAlpine, M. C. ; Friedman, R. S; Lieber, C. M. (2003). Nanoimprint Lithography for Hybrid Plastic Electronics. *Nano Lett.*, 3, 443-445, 1530-6992.

McCarthy, S. L.; Lambe, J.(1978). LEIT effect in metal-insulator-semiconductor tunnel junctions. *Appl. Phys. Lett.* 33,10, 858-860, 1077-3118.

Murukeshan, V.M; Chua, J. K.; Tan, S. K.; Lin, Q. Y. (2008) Modeling of subwavelength resist grating features fabricated by evanescent waves interference. Opt. Engi., 47, 12, 129001, 1560-2303.

Murukeshan, V.M.; Sreekanth, K. V. (2009). Excitation of gap modes in a metal particle-surface for sub-30nm plasmonic lithography. *Opt. Lett.*, 34, 845-847, 1539-4794.

Okazaki, S. (1991). Resolution limits of optical lithography. *J. Vac. Sci. Technol.* B, 9, 2829-2833, 1520-8567.

Palik, E. D. (1985). *Handbook of Optical Constants of Solids.* Academic Press, 0125444222, Orlando.

Prodan, L.; Euser, T. G; Wolferen, V.; Beigang, R.; Kuipers.L. (2004) Large-area two-dimensional silicon photonic crystals for infrared light fabricated with laser interference lithography. *Nanotechnology*, 5, 639-642, 1361-6528.

Raether, H. (1988). *Surface plasmons on smooth and Rough Surfaces and on Gratings.* Springer, 978-3-540-17363-2, Berlin Heidelberg.

Rendell, R.W.; Scalapino, D. J.; Muhlschlegel, B. (1978). Role of local plasmon modes in light emission from small-particle tunnel Junctions, *Phys. Rev. Lett.*, 41, 25, 1746-1750, 1079-7114.

Rendell, R.W.; Scalapino, D. J. (1981). Surface plasmons confined by microstructures on tunnel junctions. *Phys. Rev. B,* 24, 6, 3276-3294, 1550-235X.

Scheckler, E. W.; Tam, N. N.; Pfau, A. K.; Neureuther, A. R. (1993). An efficient volume removal algorithm for practical three dimensional lithography simulation with experimental verification", *IEEE Trans. Comput-Aided Des.* 12, 1345, 0278-0070.

Sethian, J. A.; Adalsteinsson. (1997). An overview of level set methods for etching, deposition and lithography development. *IEEE Trans. Semicond. Manuf.*, 10, 167-184, 0894-6507.

Shao, D. B.; Chen, S. C. (2005). Surface plasmon assisted nanoscale photolithography by polarized light, *Appl. Phys. Lett,* 86, 253107 (1-3), 1077-3118.

Silverman, J. P. (1998). Challenges and progress in x-ray lithography. *J. Vac. Sci. Technol.* B, 16, 3137-3141, 1520-8567.

Srituravanich, W.; Fang, N.; Sun, C.; Luo, Q.; Zhang, X. (2004). Plasmonic nanolithography. *Nano Lett.*, 4, 6, 1085-1088, 1530-6992

Stockman, M. (2008). Spasers explained, *nature photonics*, 2 , 327-329, 1749-4893.

Wu, Q; Feke, G. D.; Grober, R.D.; Ghislain, L. P. (2007). Realization of numerical aperture 2.0 using a gallium phosphide solid immersion lens. *Appl. Phys. Lett.*, 75, 4064-4067, 1077-3118.
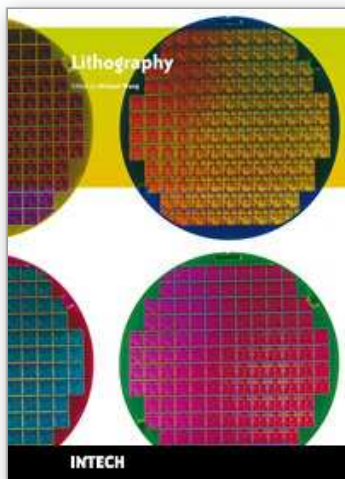
Lithography

Edited by Michael Wang

ISBN 978-953-307-064-3

Hard cover, 656 pages

Publisher InTech

Published online 01, February, 2010

Published in print edition February, 2010

Lithography, the fundamental fabrication process of semiconductor devices, plays a critical role in micro- and nano-fabrications and the revolution in high density integrated circuits. This book is the result of inspirations and contributions from many researchers worldwide. Although the inclusion of the book chapters may not be a complete representation of all lithographic arts, it does represent a good collection of contributions in this field. We hope readers will enjoy reading the book as much as we have enjoyed bringing it together. We would like to thank all contributors and authors of this book.

INTECH

open science | open minds